JOURNAL OF VIROLOGY, Mar. 2004, p. 2382–2393 Vol. 78, No. 5
0022-538X/04/$08.00+0 DOI: 10.1128/JVI.78.5.2382–2393.2004
Copyright © 2004, American Society for Microbiology. All Rights Reserved.

The Matrix Protein of Marburg Virus Is Transported to the Plasma Membrane along Cellular Membranes: Exploiting the Retrograde Late Endosomal Pathway

Larissa Kolesnikova, Sandra Bamberg, Beate Berghöfer, and Stephan Becker*

Institut für Virologie der Philipps-Universität Marburg, D-35037 Marburg, Germany

Received 3 September 2003/Accepted 14 November 2003

VP40, the matrix protein of Marburg virus, is a peripheral membrane protein that has been shown to associate with membranes of multivesicular bodies (MVBs) (L. Kolesnikova, H. Bugany, H.-D. Klenk, and S. Becker, J. Virol. 76:1825–1838, 2002). The present study revealed that VP40 is bound to cellular membranes rapidly after synthesis. Time course studies were performed to trace the distribution of VP40 during the course of expression. First, VP40 was homogenously distributed throughout the cytoplasm, although the majority of protein (70%) was already membrane associated. Next, VP40 accumulated in MVBs and in tubular protrusions emerging from MVBs. Finally, VP40 appeared in a patch-like pattern beneath the plasma membrane. These morphological results were supported by iodixanol density gradient analyses. The majority of VP40-positive membranes were first detected comigrating with small vesicles. VP40 was then shifted to fractions containing endosomal marker proteins, and later, to fractions containing plasma membrane marker proteins. Blocking of protein synthesis by use of cycloheximide at the time when VP40 was mainly associated with the small vesicles did not prevent the redistribution of VP40 to the late endosomes and further to the plasma membrane. The inhibition of intracellular vesicular trafficking by monensin significantly reduced the appearance of VP40 at the plasma membrane. In conclusion, we suggest that the transport of the Marburg virus matrix protein VP40 involves its accumulation in MVBs followed by the redistribution of VP40-enriched membrane clusters to the plasma membrane.

It is currently believed that the matrix (M) proteins of enveloped viruses connect the genome-enwrapping nucleocapsids with the viral surface and play a key role in the viral budding process (17). This is underscored by the finding that the release of recombinant viruses with deleted M proteins is drastically reduced (9, 36).

In infected cells, the M proteins of negative-strand RNA viruses are detected in a soluble form but are also found in association with the viral nucleocapsids and with cellular membranes (17, 32). The intracellular transport of M proteins to the sites of budding is not well investigated. For some viruses that bud at the plasma membrane, it has been suggested that the M proteins reach their target by comigration together with the respective viral surface proteins (36, 47–49). In most cases, however, singly expressed M proteins seem to be transported to the plasma membrane independently of other viral components. This was concluded from the finding that recombinantly expressed M proteins are released into the supernatant in a membrane-associated form (21–23, 25, 33, 53). Spatiotemporal aspects of independent transport of M proteins to the plasma membrane are poorly understood.

Marburg virus (MARV), a filovirus, is the causative agent of a fatal hemorrhagic fever that causes sporadic outbreaks in central Africa (60). To date, neither a vaccine nor a treatment for the MARV infection is available. The filamentous enveloped MARV particles are composed of seven structural proteins and a negative-sense RNA genome (12). The genome is enwrapped by the nucleocapsid complex, which has four protein constituents, NP, VP35, L, and VP30 (6). Between the nucleocapsid and the lipid envelope, two proteins are detected, the matrix protein VP40 and VP24, whose function is elusive. Inserted into the viral lipid envelope is the transmembrane glycoprotein GP, which mediates the recognition of target cells.

Members of our laboratory have investigated the intracellular distribution of the matrix protein VP40 in MARV-infected cells and reported recently that a small part of VP40 was associated with the nucleocapsids, while the majority was associated with cellular membranes (30). High concentrations of VP40 were observed in patches at the plasma membrane, where budding of progeny viruses took place, and in foci of plasma membrane proliferation that were devoid of nucleocapsids. Additionally, VP40-enriched multivesicular bodies (MVBs) were found that represent the late endosomal compartment. VP40-positive MVBs were detected in the perinuclear region and beneath the plasma membrane. Upon recombinant expression, VP40 was located in MVBs, in patches beneath the plasma membrane, and in plasma membrane protrusions. The detected VP40-positive membrane structures contained marker proteins of the late endosome or lysosome, e.g., lysosome-associated membrane protein 1 (Lamp-1). MVBs function as a sorting compartment in which proteins destined for degradation are sorted away from proteins that are recycled to the Golgi apparatus or to the plasma membrane (retrograde endosomal pathway) (for reviews, see references 20 and 46). The goal of the present study was to elucidate whether

* Corresponding author. Mailing address: Institut für Virologie der Philipps-Universität Marburg, Robert-Koch-Strasse 17, D-35037 Marburg, Germany. Phone: 49 6421-2865433. Fax: 49 6421-2865482. E-mail: becker@staff.uni-marburg.de.

MARV VP40 utilizes the retrograde endosomal pathway for its transport to the sites of budding at the plasma membrane.

Here we show that VP40 is associated with cellular membranes early after synthesis and accumulates first in MVBs of different morphology before it appears in clusters beneath the plasma membrane. While the intracellular distribution of VP40 changed, the percentage of VP40 that was bound to membranes remained constant, at approximately 80%. Studies of the localization of VP40 in the presence of drugs (monensin and NH_4Cl) that are known to impair intracellular vesicular trafficking and lysosome function showed that the delivery of VP40 to late endosomes is essential for its redistribution to the plasma membrane. Taken together, the results of the present study highlight a novel pathway for a viral matrix protein that requires association with the late endosome for its transport to the plasma membrane.

MATERIALS AND METHODS

Materials. Cycloheximide was used at 100 μg/ml, and monensin was used at 10 μM. Reagents were purchased from Sigma-Aldrich. Horseradish peroxidase (HRP) (type II; Sigma-Aldrich) was used at 5 mg/ml. Transferrin conjugated with tetramethylrhodamine (Molecular Probes, Leiden, The Netherlands) was used at 50 μg/ml. For the identification of MARV VP40, a mouse monoclonal antibody (kindly provided by the Centers for Disease Control and Prevention, Atlanta, Ga.) and affinity-purified rabbit serum against VP40 were used. For the identification of BiP/GRP78, Lamp-1, integrin alpha 2 (VLA-2a), GM130 (Golgi compartment), and Rab11, we used monoclonal antibodies from Transduction Laboratories (BD, Heidelberg, Germany). Secondary antibodies conjugated with fluorescein isothiocyanate or rhodamine (for immunofluorescence), with HRP (for Western blotting), or with colloidal gold (for immunoelectron microscopy) were from Dianova (Hamburg, Germany) or from Dako A/S (Copenhagen, Denmark).

Viruses and cell lines. The Musoke strain of MARV, isolated in 1980 in Kenya (50), was propagated in C1008 cells and purified as described previously (16). The recombinant vaccinia virus MVA-T7 was grown and titrated in chicken embryo fibroblasts as described by Sutter et al. (52). C1008, a monkey kidney cell line, HUHT-7, a human hepatoma cell line, and HeLa cells were cultured in Dulbecco's modified Eagle medium (DMEM) containing 10% fetal calf serum, a penicillin-streptomycin solution, and 2% L-glutamine. The cells were incubated at 37°C in 5% CO_2. The culture medium for HUHT-7 cells was additionally supplemented with 0.5 mg of Geneticin per ml. Infection and transfection of HeLa cells were carried out as described earlier (37).

Molecular cloning. For generation of a plasmid encoding VP40, the region encompassing nucleotides 4565 to 5959 of the Marburg virus genome (EMBL Nucleotide Sequence Database accession number Z12132) was amplified by reverse transcriptase PCR using primers which facilitated cloning of the resulting PCR fragment into the *Bam*HI restriction endonuclease site of the vector pTM1 (15). The resulting plasmid was designated pTM-VP40. Plasmids encoding fusion proteins of VP40 with green fluorescent protein (GFP) were constructed by using the plasmid pTM-eGFP. pTM-eGFP contained the open reading frame of enhanced GFP in the *Bam*HI/*Spe*I site of pTM1 under the control of the T7 promoter. Due to the cloning procedure, the *Bam*HI and *Spe*I sites were destroyed. For construction of a plasmid encoding a GFP fusion protein with VP40 at the C terminus, the open reading frame of VP40 (nucleotide positions 4568 to 5479 of the viral genome) was amplified from plasmid pTM-VP40 with primers enabling the cloning of the resulting PCR fragment into the *Pst*I and *Sal*I restriction sites of the vector pTM-eGFP. The resulting vector was designated pTM-GFP-VP40. For generation of a vector encoding a fusion protein with GFP at the C terminus, the open reading frame of VP40 was amplified from pTM-VP40 as a template and was cloned into *Eco*RI- and *Sac*I-cleaved pTM-eGFP. The resulting vector was designated pTM-VP40-GFP. The vector pTM-$VP40_{M11A}$, in which methionine at amino acid position 11 was mutated to alanine, was constructed by site-directed mutagenesis, exchanging A at position 4598 to G and T at position 4599 to C, with the vector pTM-VP40 as a template.

The vector pCAGGS-VP40 was generated by a PCR amplifying the open reading frame of VP40 from the plasmid pTM-VP40. The resulting fragment contained a *Sma*I site at the 5′ end and a *Not*I site at the 3′ end. This fragment was cloned into vector pCAGGS that was cut with *Eco*RI, treated with Klenow polymerase in the presence of deoxynucleoside triphosphates, and then digested with *Not*I.

Transfection of HUHT-7 and HeLa cells and subcellular fractionation. HUHT-7 cells were transfected with pCAGGS-VP40 by use of Lipofectamine Plus reagent according to the manufacturer's instructions. Subconfluent HeLa cells (5×10^5 cells in 7-cm^2 wells) were infected and transfected as described previously (30). Cells were washed three times with lysis buffer 1 (10 mM Tris [pH 7.5], 0.25 M sucrose, 1 mM EDTA, 200 μM orthovanadate, and 1 mM phenylmethylsulfonyl fluoride) at 4°C, scraped off the dish in a minimal volume of lysis buffer 1, aspirated with a syringe, and destroyed by passaging 10 times through a needle (24 gauge). Nuclei were pelleted at $800 \times g$ for 5 min at 4°C. The supernatant was subjected to subcellular fractionation in discontinuous sucrose gradients (30) or in iodixanol gradients according to the method of Yeaman et al. (62), with some modifications. Briefly, the separation of different membrane compartments was achieved by centrifugation of three-step 10 to 20 to 30% (wt/vol) iodixanol gradients. One third of the cellular lysate was mixed with Opti-Prep (60% [wt/vol]), iodixanol (Sigma), and lysis buffer 1 to generate solutions containing 10, 20, or 30% iodixanol. Equal volumes of these three solutions were layered in centrifuge tubes, and samples were centrifuged at $353{,}000 \times g$ for 3 h at 4°C. Fractions (150 μl) were collected and proteins were separated by sodium dodecyl sulfate-polyacrylamide gel electrophoresis (SDS-PAGE) and immunoblotted. The densities of the fractions were determined by measuring their respective refractive indexes (13).

Western blot analysis. Western blot analysis was carried out as described previously (5). The antibodies used and their respective dilutions are given in the figure legends.

Radioactive metabolic labeling and immunoprecipitation analysis. At the indicated times after transfection, cells were starved for 1 h with methionine- and cysteine-deficient DMEM. The medium was removed, and cells in a six-well plate (7 cm^2 per well) were labeled with 50 μCi of [^{35}S] Promix (Amersham) per dish for 30 min in 1 ml of starvation medium. After metabolic labeling, cells were washed with DMEM and incubated for the indicated chase period or were lysed immediately. For cell lysis, cells were washed three times with lysis buffer 1 at 4°C, scraped off the dish in a minimal volume of lysis buffer 1, and lysed by 10 strokes through a 24-gauge cannula. The postnuclear fraction was subjected to a flotation assay as described previously (30). Fractions were collected from the top. Each fraction was resuspended in an equal amount of 2× ice-cold lysis buffer 2 (1× lysis buffer 2 is 20 mM Tris-HCl [pH 7.5], 100 mM sodium chloride, 0.4% [wt/vol] deoxycholic acid, 0.5% [wt/vol] NP-40, and 5 mM EDTA) and was incubated for 1 h at 4°C with 30 μl of protein A-Sepharose which had been equilibrated in lysis buffer 2. Sepharose beads were precipitated at $8{,}500 \times g$ for 2 min at 4°C, and supernatants were further incubated for 1 h with 1 μl of an anti-VP40 mouse monoclonal antibody. Immune complexes were bound to 30 μl of protein A-Sepharose for 1 h at 4°C, precipitated, and washed three times with ice-cold lysis buffer 2. The final pellets were resuspended in 30 μl of sample buffer (20% glycerin, 4% SDS, 100 mM Tris-HCl [pH 6.8], 10% mercaptoethanol, 5% saturated bromphenol blue solution) and incubated for 5 min at 95°C. Fifteen microliters of [^{35}S] Promix-labeled sample was subjected to SDS-PAGE. The radioactive signals were visualized by exposing dried gels to a BioImager plate and were quantified by using a bioimaging analyzer (BAS-1000; Fuji) with Raytest TINA software.

Indirect immunofluorescence and immunoelectron microscopic analyses. HeLa and HUHT-7 cells expressing VP40 were fixed with 4% paraformaldehyde at the indicated times. Subsequent immunofluorescence analysis was performed as described previously (6). For determination of the percentage of VP40-positive cells that contained VP40 bright spots or clusters in the perinuclear region and/or close to the plasma membrane, 6 to 10 randomly chosen regions were photographed (×40 objective; each region contained 6 to 18 cells). Cells expressing VP40 were differentiated into two classes, those that contained VP40 in the perinuclear region (bright spots or tubular network) and those that contained VP40 adjacent to the plasma membrane. The weighted mean value and the standard deviation were determined on a per field basis. For immunoelectron microscopy, cells were fixed with 4% paraformaldehyde. The fixative was removed and free aldehydes were quenched with 50 mM NH_4Cl in phosphate-buffered saline (PBS). After dehydration, samples were embedded in LR Gold (31). Indirect immunogold labeling was carried out with ultrathin sections. The antibodies used and their respective dilutions are given in the figure legends. For immunoelectron microscopic analysis of VP40-positive membranes, we used the membrane-containing fraction from the flotation analysis. Additionally, viral envelopes that had been removed by detergent treatment of MARV particles as described previously (30) were analyzed. A drop of the analyzed suspension was deposited on Formvar-carbon-coated nickel grids for 1 min. The excess fluid was blotted away with Whatman filter paper, and the grids were floated on a drop of

PBS containing 1% bovine serum albumin for 10 min. Indirect immunostaining was performed by incubation with an anti-VP40 mouse monoclonal antibody for 60 min, and bound antibodies were detected with a donkey anti-mouse immunoglobulin G (IgG) antibody coupled to 6-nm-diameter gold particles (Dianova). After being washed with PBS, the samples were negatively stained with 2% phosphotungstic acid and examined in a Zeiss 109 electron microscope. For the quantification of gold particles in the VP40-positive structures, 10 micrographs were taken at a primary magnification of ×50,000. The density of gold labeling at the surfaces of profiles of VP40-positive structures was determined by morphometric methods (59). Micrographs were scanned by using Leafscan 45 software, and the surfaces of the profiles of VP40-positive structures were determined by using Raytest TINA software.

RESULTS

VP40 associates with cellular membranes early after synthesis. VP40 is a peripheral membrane protein whose interaction with membranes is resistant to high salt conditions, EDTA treatment, and high pHs (30). To analyze the kinetics of membrane binding, we performed pulse-chase analyses of VP40-expressing HeLa cells and determined the membrane binding status of VP40 by a subsequent flotation analysis (7). Under the chosen conditions, membrane-associated proteins floated from the dense sucrose fractions (fractions 4 to 6) to the 10 to 45% interface (fraction 2). Figure 1A shows that approximately 25% of the VP40 was bound to membranes directly after the radioactive pulse (Fig. 1B, fraction 2, white bar). At 2 h chase, the membrane-bound portion of VP40 was increased to 55% (Fig. 1A and B, fraction 2, black bar). Thus, VP40 became associated with cellular membranes early after synthesis with kinetics that were similar to those for the influenza A virus matrix protein (63). The membrane association of VP40 was also determined by Western blotting at 6, 12, and 18 h posttransfection. It was found that approximately 80% of the VP40 was constantly bound to membranes. Flotation of VP40 was abolished in the presence of 1% Triton X-100 (not shown). The flotation assay was controlled by using the cellular transmembrane protein Lamp-1 (not shown). Taken together, these results indicate that the membrane association of VP40 takes place rapidly after synthesis, reaching plateau levels of approximately 80%. The expression of VP40 was performed by using the recombinant vaccinia virus MVA T7, which is widely used to study the pathways of recombinant proteins because of its superior expression efficiency (52). This system was successfully used for the study of viral M proteins (22), glycoproteins (58), and nucleocapsid proteins (6). However, considering the large number of proteins expressed by vaccinia virus, we tested whether the VP40 distribution was affected by these extraneous proteins. Therefore, experiments were performed in parallel in HUHT-7 cells that were transfected with the plasmid pCAGGS-VP40, which contains the VP40 open reading frame under the control of the beta-actin promoter (29, 40). The cells were subjected to a flotation assay under the pulse-chase conditions described above. We found that the kinetics of membrane association of VP40 in HUHT-7 cells were essentially the same as those in HeLa cells (not shown).

VP40 migrated in SDS-PAGE gels as a double band, at 37 and 39 kDa (Fig. 1A). The 39-kDa form could be detected only if a large amount of protein was loaded onto the gel. Both forms were able to associate with cellular membranes. The removal of a potential second start codon at amino acid position 11 of the VP40 polypeptide chain did not abolish the appearance of VP40 as a double band (data not shown). Thus, we presumed that the double band is the result of a hitherto unidentified posttranslational modification.

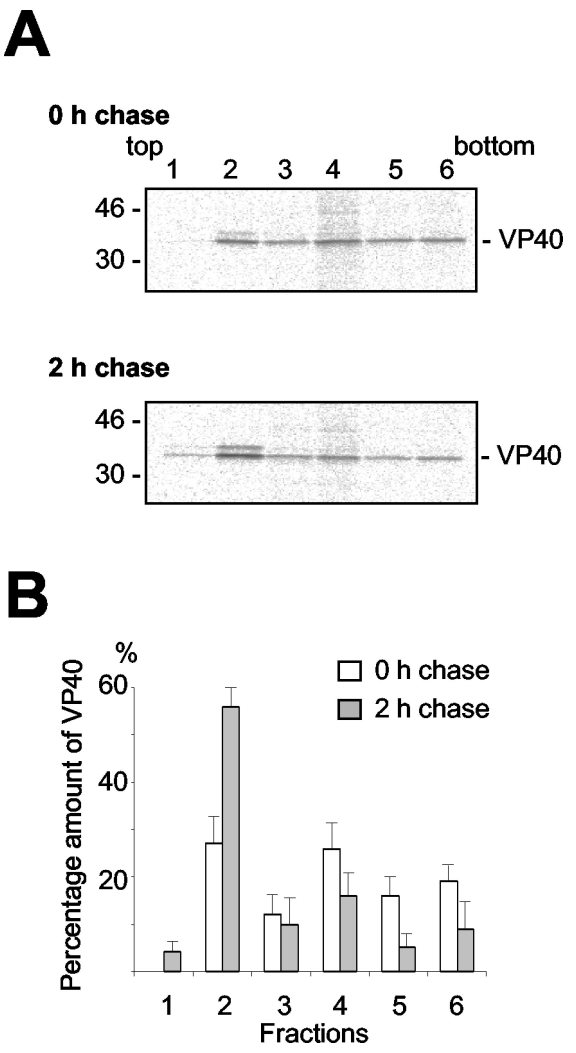

FIG. 1. Newly synthesized VP40 interacts with membranes. (A) HeLa cells expressing VP40 were pulse-labeled at 10 h posttransfection with 50 μCi of [^{35}S]Promix for 30 min. Cells were lysed either immediately after labeling (upper panel) or after a 2-h chase in DMEM (bottom panel). The postnuclear supernatant was supplemented with sucrose to give a final concentration of 63%, placed at the bottom of a centrifuge tube, and overlaid with 45 and 10% sucrose. The gradient was centrifuged to equilibrium at 40,000 rpm in an SW60 rotor. Fractions were collected from the top and subjected to immunoprecipitation with a mouse monoclonal antibody against VP40. (B) The intensities of VP40-specific signals in panel A were quantified as described in Materials and Methods. The extent of VP40 in all fractions was set to 100%. The data represent averages and standard deviations from three independent experiments.

MVBs represent places of early accumulation of VP40. Previous ultrastructural analyses showed that VP40 was associated with membranes of MVBs located in the perinuclear region and was concentrated in patches beneath the plasma membrane (30). All of the VP40-positive membrane structures contained marker proteins of the late endosome (e.g., Lamp-1), although at different concentrations. In immunofluorescence

analyses, the VP40-positive MVBs appeared as bright spots around the nucleus and/or as a tubular-like network. It was hypothesized that VP40 uses the endosomal system to be transported to the plasma membrane, where budding of progeny viruses takes place (30). To test this hypothesis, we performed a time course study of the intracellular distribution of VP40 by using immunofluorescence analysis. VP40 was again synthesized by using (i) the vaccinia virus T7 system in HeLa cells and (ii) transient expression under the control of the eukaryotic beta-actin promoter in HUHT-7 cells.

With the vaccinia virus T7 system, initial signs of VP40 expression were detected at 4 to 5 h posttransfection. At this time, VP40 was mostly diffusely distributed, and 20% of the VP40-positive cells contained, additionally, very small bright spots in the perinuclear region (Fig. 2A). In parallel, we quantified the amount of soluble and membrane-associated VP40 with a flotation assay and found that despite its predominant diffusive appearance, approximately 70% of the VP40 was already associated with membranes (Fig. 2B). At 6 h posttransfection, 41% of VP40-expressing cells contained the protein in bright spots in the perinuclear region, and in a quarter of these cells VP40 was also detected beneath the plasma membrane (Fig. 2C). At 10 h posttransfection, in 60% of VP40-expressing cells, the protein was detected in the perinuclear region (bright spots or tubular-like network), and half of these cells displayed VP40 beneath the plasma membrane (Fig. 2A and C). Notably, all of the cells with VP40 beneath the cell surface contained VP40 in the perinuclear region as well. During the course of expression, the bright spots in the perinuclear region and at the plasma membrane increased in size (Fig. 2A). VP40-positive perinuclear spots did not display uniform appearances. Some spots were rather round (Fig. 2D, left panel) and others were of irregular shapes, with single or multiple tubular-like protrusions (Fig. 2D, right panel). This result suggested that the VP40-positive perinuclear spots could be reorganized during the course of expression, thereby inducing the formation of a VP40-positive tubular-like network.

The VP40 distribution in HUHT-7 cells was similar to that with the vaccinia virus expression system; however, the accumulation of VP40 was slower and the VP40-positive network that was formed by tubular-like protrusions was more prominent (Fig. 2E and F). Taken together, these results show that during the course of expression, the initial diffuse appearance of VP40 is later complemented by an accumulation of VP40 around the nucleus and finally by VP40-positive spots at the plasma membrane.

We then investigated whether the perinuclear VP40-positive spots that were detected at early stages of expression do belong to the late endosomal compartment. To this end, HeLa cells expressing VP40 were loaded with a fluid phase marker (HRP) for 1 h at 2 h posttransfection and were chased for 2 to 3 h. HRP is resistant to lysosomal proteolysis and can be detected in late endosomes and lysosomes for several hours after its internalization (51). The immunofluorescence analyses showed that VP40-positive spots were colocalized with the HRP-loaded late endosomes and lysosomes (Fig. 3A, arrowheads). Colocalization of VP40 spots and markers of late endosomes (e.g., Lamp-1) was also detected in HUHT-7 cells at early stages of VP40 expression (at 8 h posttransfection) (Fig. 3B, left panels). Some of the perinuclear VP40-positive spots formed long protrusions to the cell periphery (Fig. 3B, right panels). For labeling of the early endocytic compartment (24), cells were cultured at 37°C in medium containing tetramethylrhodamine-labeled transferrin for 10 min before fixation. The VP40-containing perinuclear spots were distinct from transferrin-containing early endosomes (Fig. 3C).

According to our assumption, VP40 is transported to the plasma membrane in association with late endosomes. Thus, we analyzed whether VP40-positive late endosomes loaded with a fluid phase marker could be detected at the cell surface. To this end, HeLa cells expressing VP40 were loaded with HRP as described above; however, loading was performed at 12 h posttransfection. Immunoelectron analysis revealed membrane clusters beneath the plasma membrane that simultaneously contained VP40 and HRP (Fig. 4A). Tubular-like protrusions that were enriched in VP40 were detected at the cell surface and contained HRP as well (Fig. 4B and C). These data suggest that the redistribution of VP40 from the perinuclear region to the cell surface occurs in association with the late endosomal compartment.

VP40 is associated with membranes of different morphologies. A considerable amount of VP40 was already membrane associated when the appearance of the protein was still homogeneous (Fig. 1 and 2). Thus, it was assumed that in addition to the known particulate VP40-positive membrane structures (MVBs and patches at the plasma membrane), VP40 might be associated with membrane structures that display a homogeneous distribution. To identify these structures, we carried out an ultrastructural analysis of VP40-positive membranes at early stages of expression (at 6 h posttransfection). HeLa cells expressing VP40 were lysed, the postnuclear supernatant was subjected to flotation analysis, and the membrane fraction was analyzed by immunoelectron microscopy and negative staining. Additionally, immunoprecipitated VP40-positive membranes were studied with ultrathin sections. At this time, VP40 was predominantly detected at the surfaces of small vesicles with diameters of 30 to 50 nm (Fig. 5A). To identify the entire spectrum of intracellular VP40-positive membrane structures, we performed an ultrastructural analysis of VP40-positive membranes at later stages, when the expression level of VP40 was sufficiently high. We identified different VP40-positive membrane structures in the cell lysates. (i) VP40 was found in association with MVBs (250 to 1,000 nm in diameter; Fig. 5B to F) that displayed a patch-like distribution of VP40. Judging by the intensity of gold labeling, the surfaces of MVBs contained only small amounts of VP40 (Fig. 5B and C). The tubular- or bud-like protrusions, however, were highly enriched in VP40 (Fig. 5D to F). (ii) Very strong gold labeling was found in membrane sheets of variable size which were obviously partly destroyed during purification (Fig. 5G). The maximal size of VP40-enriched membrane sheets was 0.5 μm^2. The density of VP40 in these membrane sheets, which was estimated by the number of gold beads, was similar to the density of VP40 in the MARV envelope (1,440 $\pm$ 310 per μm^2 versus 1,300 $\pm$ 120 per μm^2) (not shown). This finding suggested that VP40 was able to form membrane-associated submicron-scale clusters independently of nascent viral RNA and other viral proteins. Most likely, VP40 became concentrated in the tubular extensions of the MVBs, resulting in the detected membrane patches that contained high amounts of VP40.

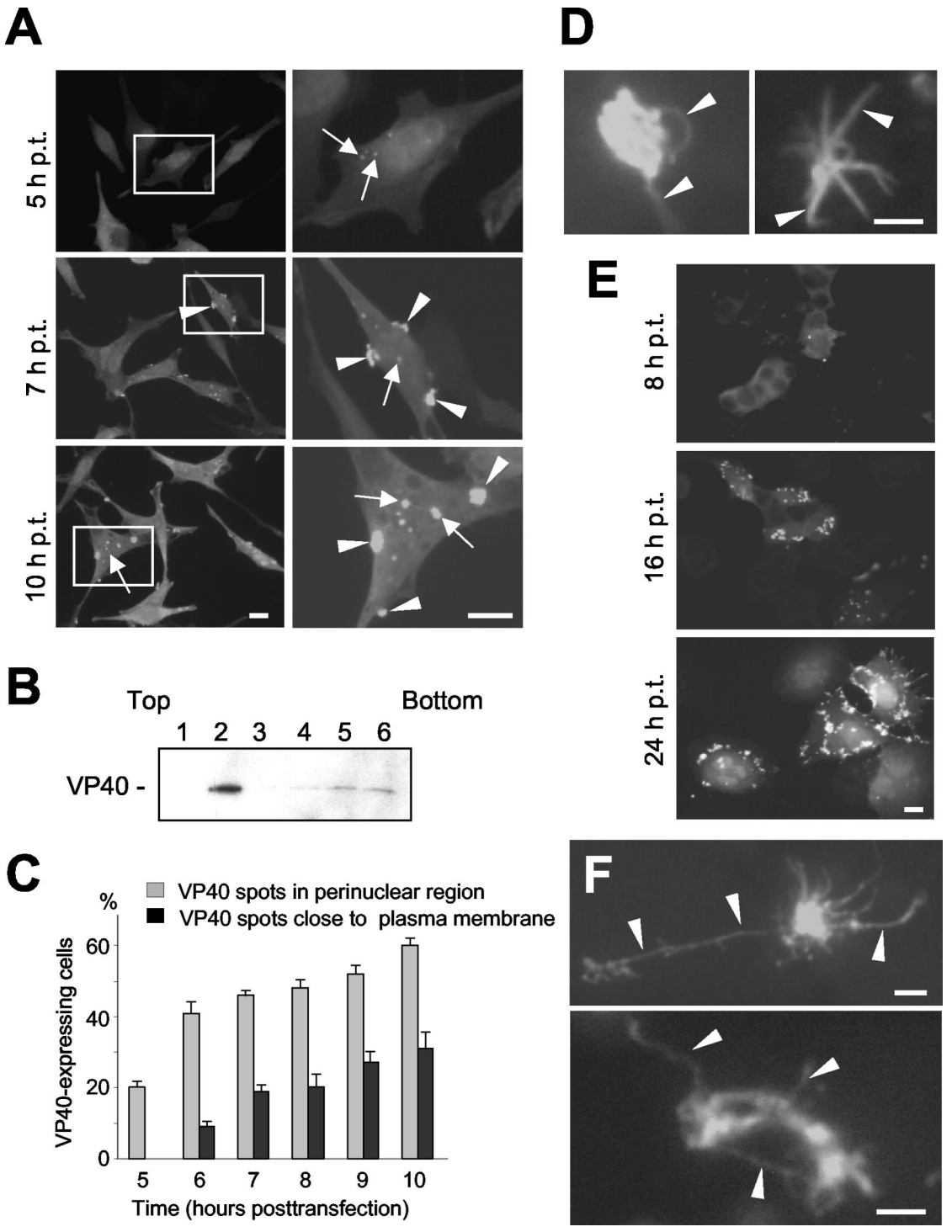

FIG. 2. Time course study of intracellular distribution of VP40. (A) HeLa cells expressing VP40 were fixed with 4% paraformaldehyde at different times posttransfection. Cells were immunostained with an anti-VP40 monoclonal antibody (dilution, 1:100) and a secondary donkey anti-mouse IgG conjugated with rhodamine (dilution, 1:100). Left panels, cells at 5, 7, and 10 h posttransfection (magnification, ×40); right panels, enlarged images of framed cells. Arrows, VP40 in perinuclear bright spots; arrowheads, VP40 in bright spots beneath the plasma membrane. (B) Flotation assay of HeLa cells expressing VP40 at 5 h posttransfection. The gradient was fractionated from the top, and samples were separated by SDS-PAGE and blotted onto a polyvinylidene difluoride membrane. The membrane was stained with an anti-VP40 monoclonal antibody (dilution, 1:1,000). Top of the gradient, fraction 1; bottom of the gradient, fraction 6. (C) Percentages of VP40-expressing HeLa cells which contained perinuclear bright spots (gray bars) and VP40 bright spots beneath the plasma membrane (black bars). (D) VP40 bright spots with single and multiple tubular-like protrusions (arrowheads) in HeLa cells at 10 h posttransfection with pTM-VP40. (E) HUHT-7 cells expressing VP40 were fixed with 4% paraformaldehyde at 8, 16, and 24 h posttransfection and were immunostained as described above (magnification, ×40). (F) VP40 bright spots with multiple tubular-like protrusions (arrowheads) in HUHT-7 cells at 16 h posttransfection with pCAGGS-VP40. Bar, 10 μm (A and E) or 2 μm (D and F).

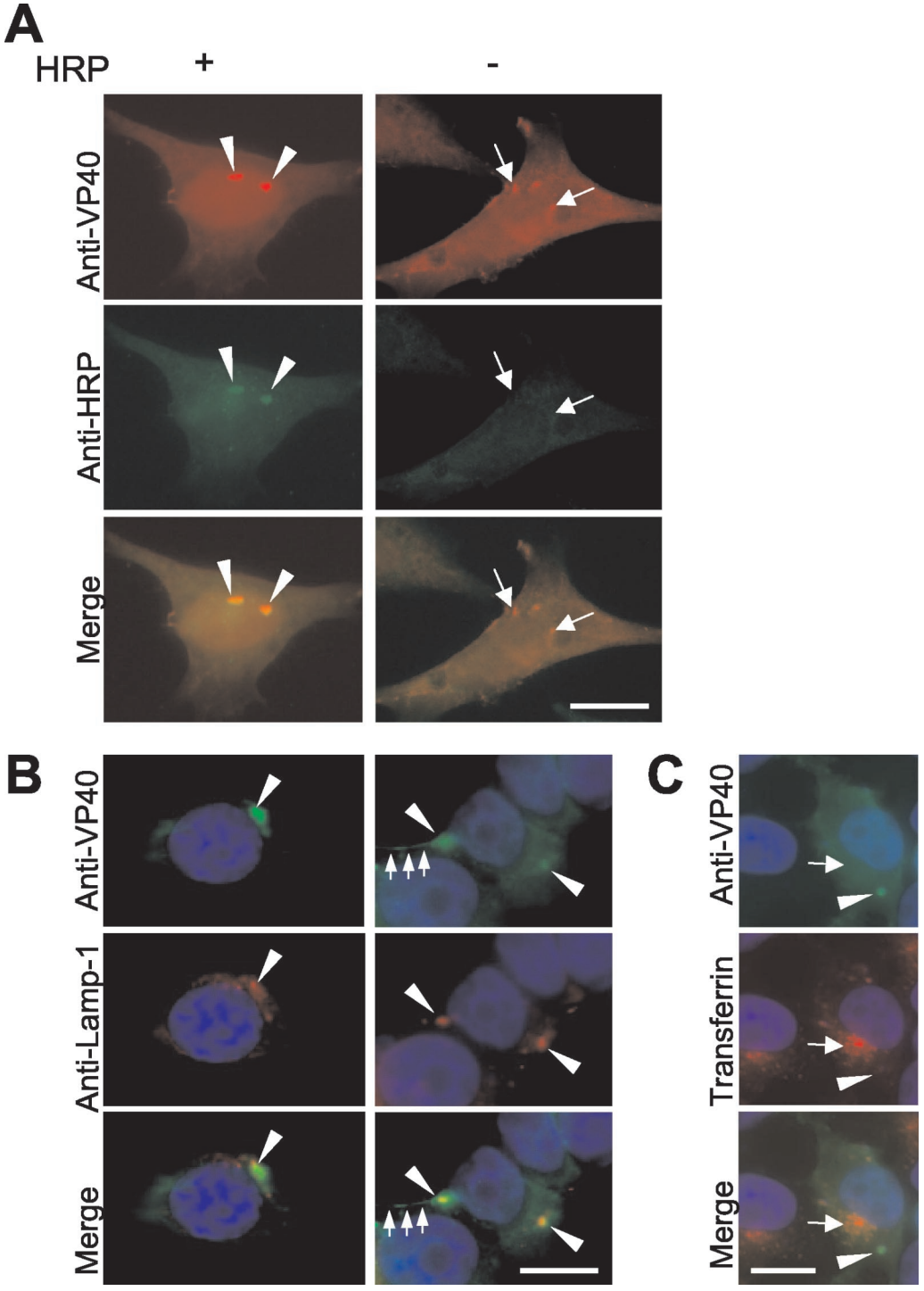

FIG. 3. VP40 is colocalized with the endosomal-lysosomal compartment early after synthesis. (A) VP40-expressing HeLa cells were loaded with the fluid phase marker HRP for 1 h at 2 h posttransfection and were chased for an additional 2 h (+) or were not loaded with HRP (−). Double immunofluorescence staining was performed with a rabbit anti-HRP antibody (1:50) and a mouse anti-VP40 antibody (1:100). Arrowheads, colocalization of VP40 and HRP; arrows, VP40 bright spots that are not colocalized with HRP. (B) VP40-expressing HUHT-7 cells were fixed at 7 h posttransfection and double immunostained with an anti-VP40 rabbit polyclonal antibody (dilution, 1:100) and a mouse anti-Lamp-1 monoclonal antibody (dilution, 1:50). Nuclei were counterstained with DAPI (4′,6′-diamidino-2-phenylindole). Arrowheads, colocalization of VP40 and Lamp-1; arrows, long tubular VP40-positive extensions. (C) VP40-expressing HUHT-7 cells were incubated with transferrin conjugated with tetramethylrhodamine for 10 min before fixation. Fixation was done at 7 h posttransfection. Arrowheads, localization of VP40 spots; arrows, localization of transferrin. Bar, 10 μm.

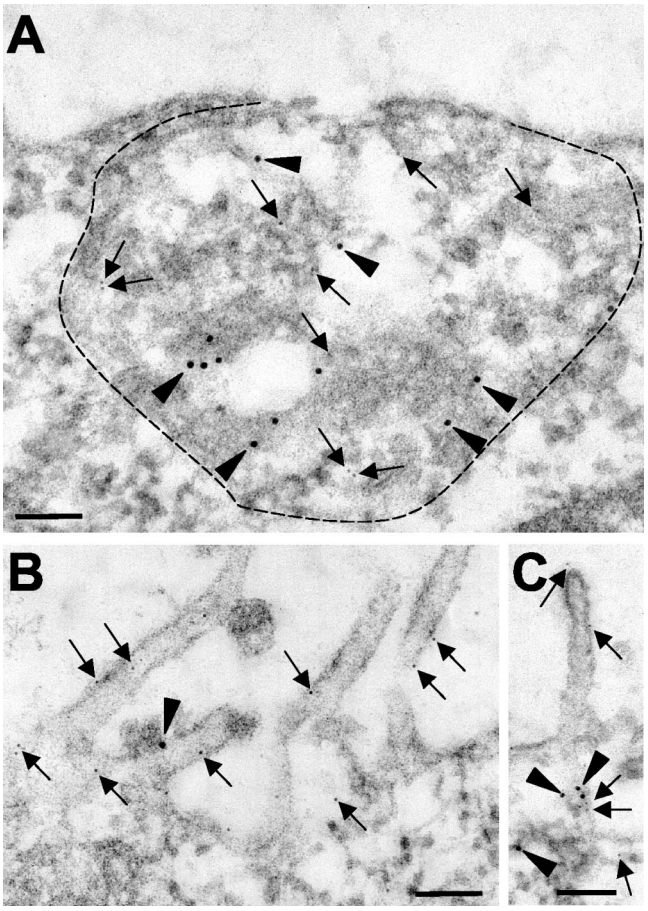

FIG. 4. Immunoelectron microscopic analysis of VP40-expressing HeLa cells loaded with fluid phase marker. VP40-expressing HeLa cells were loaded with the fluid phase marker HRP for 1 h at 12 h posttransfection, washed, and chased for an additional 2 to 3 h. After fixation with 4% paraformaldehyde, cells were dehydrated and embedded in LR Gold. Double immunostaining of ultrathin sections was performed with a rabbit anti-HRP antibody (12-nm-diameter gold beads; arrowheads) and a mouse anti-VP40 antibody (6-nm-diameter gold beads; arrows). (A) VP40-positive membrane cluster beneath the plasma membrane (highlighted by dashed line). (B and C) VP40-positive tubular-like protrusions at the cell surface. Bar, 100 nm.

Trafficking of VP40 between cellular compartments. To support the hypothesis that VP40 is intracellularly transported via membrane-associated transport involving the late endosome, we investigated whether the sequential targeting of different membrane compartments by VP40 could be detected by density gradient centrifugation. A pilot experiment showed that the chosen method for cell fractionation, iodixanol gradients (19, 62), allows the separation of membrane proteins associated with the plasma membrane, with endoplasmic reticulum (ER)-Golgi-endosomal membranes, and with small vesicular structures (Fig. 6A). At different times posttransfection, lysates of VP40-expressing HUHT-7 cells were separated by isopycnic centrifugation through linear iodixanol gradients (Fig. 6B, top three panels). Altogether, VP40 was recovered from four peaks, which corresponded to the plasma membrane (fractions 1 to 6; peak 1), the endosomal compartment (fractions 7 to 14; peak 2), small vesicles (fractions 15 to 23; peak 3), and finally, aggregated or soluble proteins (fractions 24 to 27; peak 4) (43, 62). The migration pattern of VP40 in the gradient changed from 7 to 24 h posttransfection (Fig. 6B and C). At 7 h posttransfection, membrane-associated VP40 was recovered mainly from peak 3 (small vesicles) (Fig. 6C), with a very small amount recovered from peaks 2 and 1 (endosome-ER and plasma membrane, respectively). At 13 h posttransfection, the amount of VP40 in all fractions was increased. However, the ratio of VP40 associated with the small vesicle fractions to that in the late endosomal fractions was decreased. The same shift in ratio was detected between the small vesicle fractions and the plasma membrane fractions (Fig. 6C). This result indicates that the protein shifted from the small vesicles to the endosomal compartment and the plasma membrane (Fig. 6B and C). From 13 to 24 h posttransfection, the relative amount of VP40 in the small vesicle fraction continued to decrease, the amount in the endosomal fraction reached a plateau, and the amount at the plasma membrane increased constantly (Fig. 6B and C).

To check whether the changes in intracellular distribution of VP40 reflect a real redistribution or merely a saturation of VP40 binding sites with an accumulation of the protein in new places, we analyzed targeting of VP40 to the different membrane compartments in the presence of cycloheximide. When protein synthesis was blocked, a shift of VP40 from the small vesicle fraction to the endosomal compartment and the plasma membrane was detected (Fig. 6B, fourth panel, and C). This result pointed out that trafficking of VP40 to the plasma membrane is a complex process that involves the sequential targeting of several compartments, including the late endosome.

To further elucidate the intracellular trafficking pathways used by VP40, we treated cells transiently expressing VP40 with monensin, which blocks intracellular vesicular trafficking (27, 38). Monensin treatment resulted in an accumulation of VP40 in the bottom fractions corresponding to cytosolic or aggregated proteins. In an immunofluorescence analysis, treatment with monensin almost completely blocked the formation of VP40 spots in the perinuclear region and resulted in a bright diffuse distribution without any accumulation beneath the plasma membrane (Fig. 6B, fifth panel, and C). Taken together, these results indicate that monensin significantly reduces the association of VP40 with small vesicles and the delivery of VP40 to the late endosomes and the plasma membrane.

Cells were then treated with the weak base NH_4Cl, which raises the pH of intracellular organelles (11, 35). In comparison with the control cells at 13 h posttransfection, the relative amount of VP40 associated with small vesicles was significantly increased and the relative amount that was associated with late endosomes was decreased. As a consequence, the amount of VP40 at the plasma membrane was also reduced (Fig. 6B, sixth panel, and C).

In summary, morphological and biochemical analyses both indicated that, during the course of expression, VP40 changes its distribution in the cell. At first, VP40 appears to be membrane bound but homogeneously distributed over the cytoplasm. At the same time, the majority of VP40 migrates in the iodixanol gradient at a density that corresponds to small vesicles. VP40 then accumulates in the perinucleus in an endosomal compartment and comigrates in the iodixanol gradient with endosomal markers. Finally, VP40 arrives at the plasma

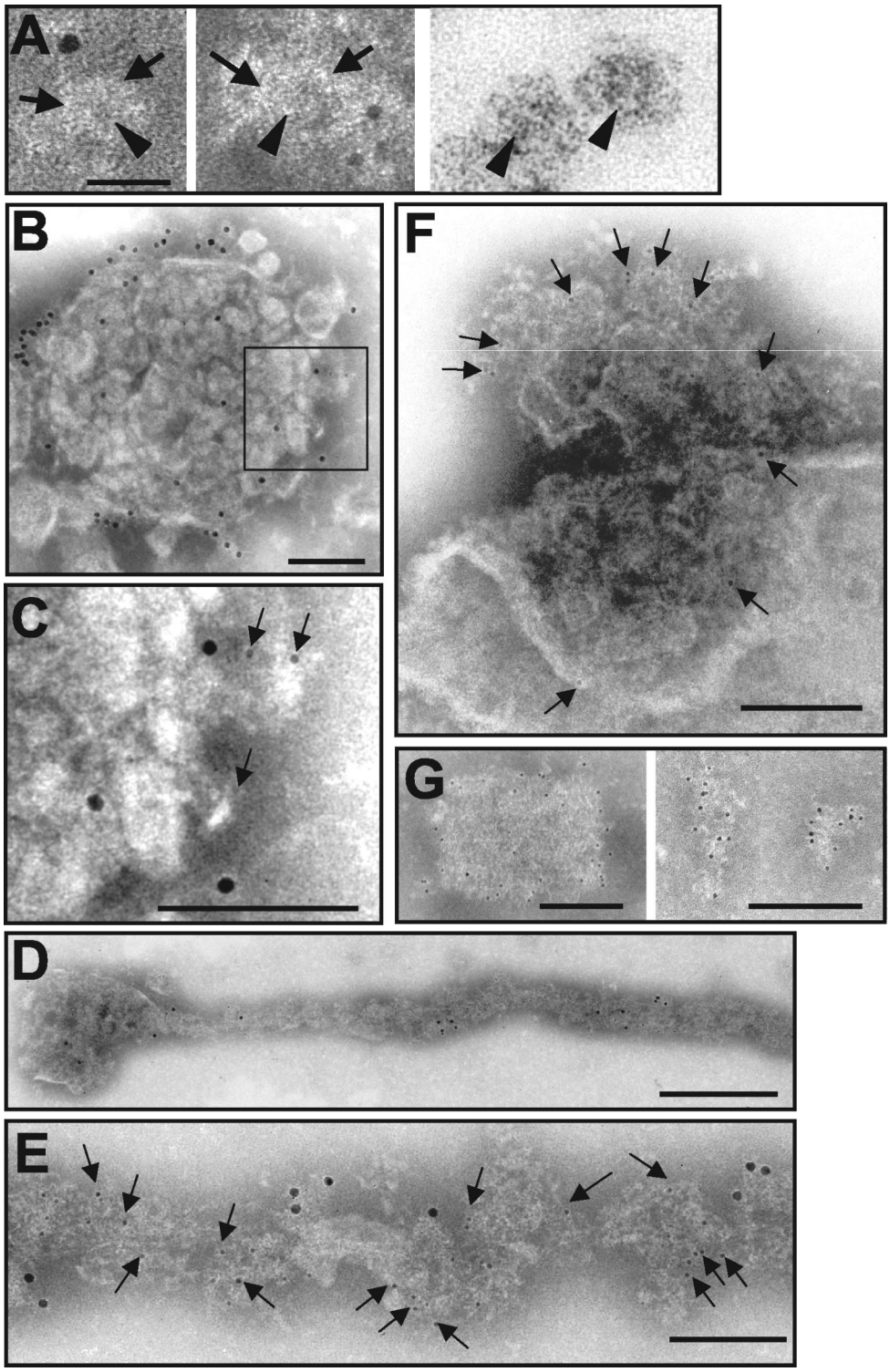

FIG. 5. Immunoelectron microscopic analysis of VP40-positive membranes purified from VP40-expressing HeLa cells by flotation assay. (A) VP40-expressing HeLa cells were lysed at 6 h posttransfection. The postnuclear supernatant was subjected to flotation analyses and the resulting membrane-containing fraction (number 2) was subjected to immunoelectron microscopy (left and middle images; VP40 is labeled with 6-nm-diameter gold beads). The right image shows small vesicles that were detected in an ultrathin section of immunoprecipitated VP40-positive membranes. Arrows, outer boundaries of small vesicles; arrowheads, inner ring-like structures. (B and C) VP40-expressing HUHT-7 cells were lysed at 24 h posttransfection. The postnuclear supernatant was subjected to flotation analyses and the resulting membrane-containing fraction (number 2) was subjected to immunoelectron microscopy. Double immunostaining was done with an anti-VP40 rabbit polyclonal antibody (12-nm-diameter gold beads) and a mouse anti-Lamp-1 monoclonal antibody (6-nm-diameter gold beads; arrows). (D, E, and F) VP40-expressing HeLa cells were lysed at 16 h posttransfection and processed as described above. Immunostaining was done with an anti-VP40 mouse monoclonal antibody (1:100) and a secondary donkey anti-mouse antibody conjugated with colloidal gold (1:40; 6-nm-diameter gold beads; arrows). Panels D and E show double immunostaining with a mouse anti-VP40 monoclonal antibody (6-nm-diameter gold beads) and a rabbit anti-actin polyclonal antibody (12-nm-diameter gold beads). (A) Small vesicles. (B) MVB. (C) Enlarged fragment of panel B. (D, E, and F) Tubular- and bud-like protrusions at the surfaces of MVBs. (E) Enlarged fragment of tubular protrusion. (G) Sheets of membrane strongly labeled with VP40. Bars, 30 nm (A), 100 nm (B, C, E, F, and G), and 400 nm (D).

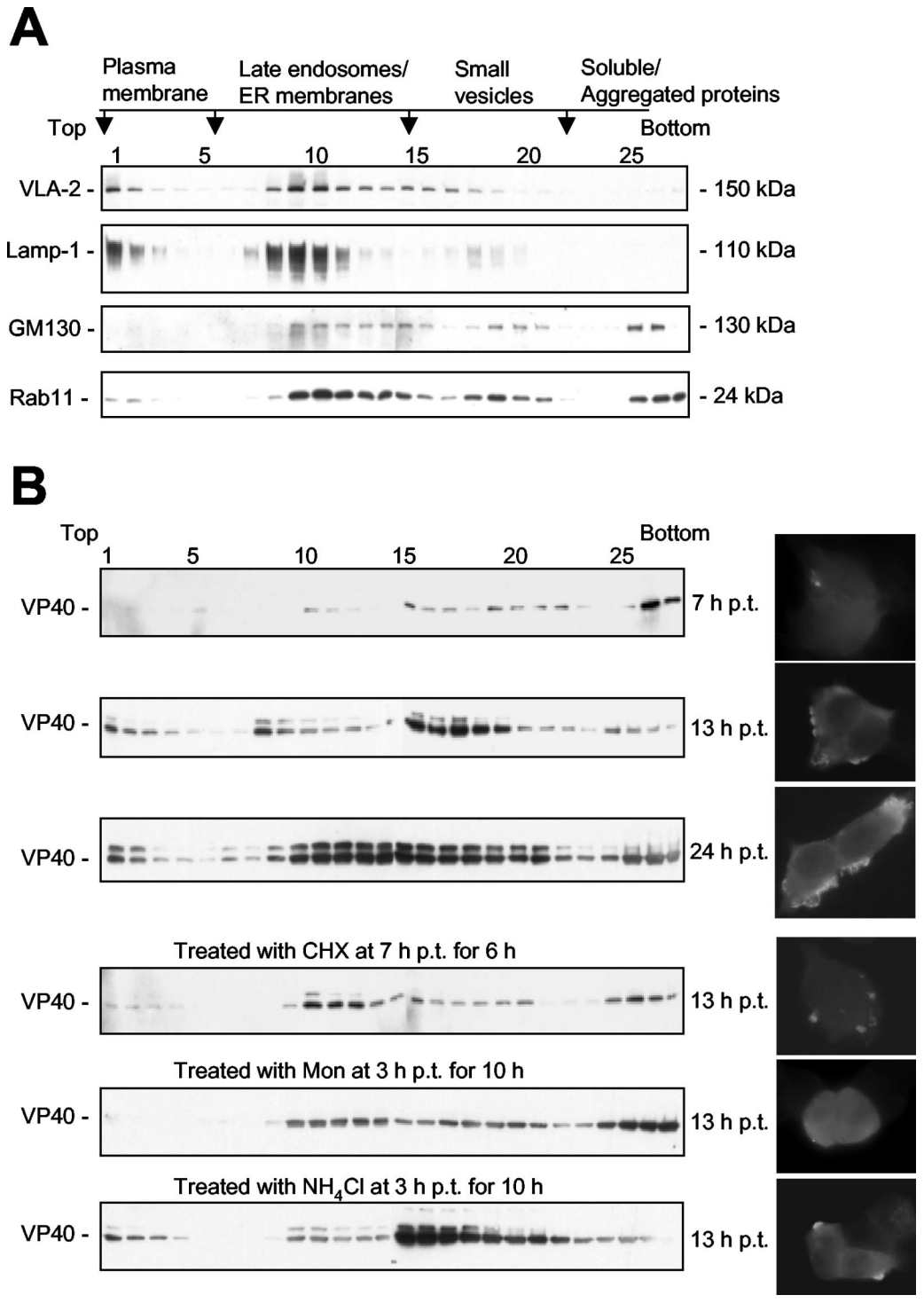

FIG. 6. Fractionation of VP40-expressing cells in an iodixanol gradient at different times posttransfection. (A) Detection of cellular proteins in the iodixanol gradients. (B) Detection of VP40 in fractions from iodixanol gradients of VP40-expressing HUHT-7 cells and immunofluorescence analysis of these cells at 7, 13, and 24 h posttransfection (top three panels). The bottom three panels show the detection of VP40 in fractions from iodixanol gradients of VP40-expressing HUHT-7 cells and immunofluorescence analysis of these cells at 13 h posttransfection in the presence of cycloheximide (CHX), monensin (Mon), or ammonium chloride (NH_4Cl). Cycloheximide (100 μg/ml) was added at 7 h posttransfection for 6 h. Monensin (10 μM) was added at 3 h posttransfection for 10 h. Ammonium chloride (10 mM) was added at 3 h posttransfection for 10 h. Positions of VP40 are indicated to the left, and times of cell harvesting are shown to the right. (C) The intensities of VP40-specific signals in the panels of Fig. 6B were quantified as described in Materials and Methods. The total amount of VP40 in all fractions was set to 100%. The graphic shows the relative amounts of VP40 as sums of fractions 1 to 6 (plasma membrane), fractions 7 to 14 (late endosomes-ER), and fractions 15 to 23 (small vesicles); for NH_4Cl-treated cells, the late endosomes-ER compartment is represented by fractions 7 to 13 and small vesicles are represented by fractions 14 to 22.

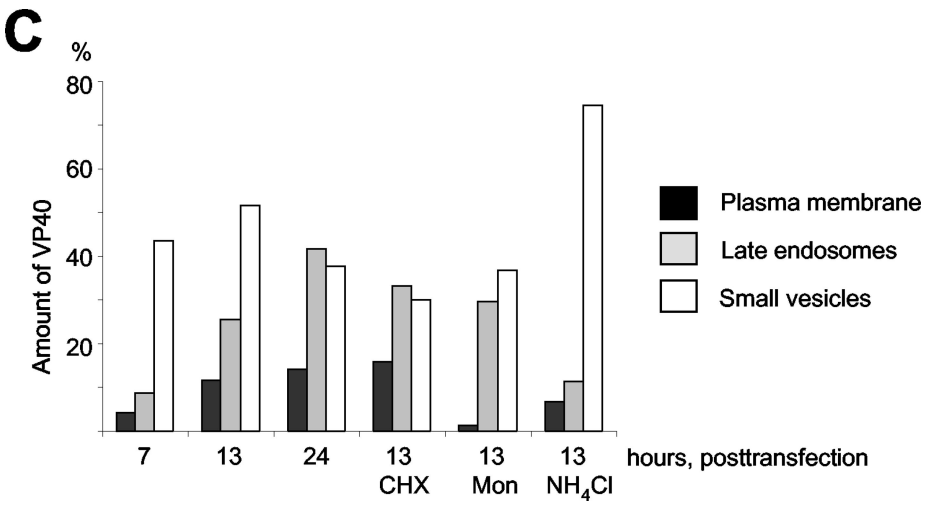

FIG. 6—*Continued.*

membrane, as shown by immunofluorescence and gradient centrifugation analysis. These data are in agreement with the assumption that the transport of VP40 to the plasma membrane takes place in association with intracellular membranes and involves the late endosomal compartment.

DISCUSSION

Despite the important role of viral matrix proteins in the assembly and release of progeny virions, it is poorly understood how these proteins are targeted to the sites of budding. Thus, we have analyzed in detail the transport of the MARV matrix protein VP40 by using a combination of time course studies and ultrastructural analyses.

We found that the primary membranes which are targeted by VP40 are vesicles with diameters of approximately 30 to 50 nm. The identity of these vesicles is still unclear. They neither were coated by a protein shell, like clathrin-coated vesicles, nor contained detectable amounts of the late endosomal marker Lamp-1.

VP40 next accumulated in the perinuclear region in association with MVBs. Finally, VP40 was found in the periphery of the cell, suggesting that the accumulation of VP40 in the late endosomal compartment represents an intermediate step during the course of its delivery to the plasma membrane. In addition, if VP40 is expressed as an N-terminal GFP fusion protein, it is still associated with membranes but cannot accumulate in MVBs (data not shown). This fusion protein is also unable to target the plasma membrane. Thus, the association of VP40 with the late endosomal compartment seems to be critical for its transport to the plasma membrane.

Studies on the distribution of VP40 in the presence of cycloheximide and monensin showed that the accumulation of VP40 in MVBs is essential for its transport to the plasma membrane. The block of protein synthesis did not prevent the redistribution of VP40 to the late endosomes and further to the plasma membrane. In contrast, the redistribution of VP40 from the small vesicles to the late endosomes and to the plasma membrane was more pronounced. This result strongly supports the hypothesis that VP40 is transported in association with intracellular membranes. This is additionally underscored by the result that inhibition of intracellular vesicular trafficking by monensin significantly reduced the appearance of VP40 at the plasma membrane. When lysosomal functioning was impaired, the relative amount of VP40 associated with small vesicles was increased and the relative amount of VP40 in late endosomes and at the plasma membrane was decreased. This result suggests that alkalization of endosomes and lysosomes has an impact on the fusion and/or fission of VP40-containing small vesicles with and from the late endosomal compartment.

Although lysosomes and late endosomes are predominantly involved in the degradation of proteins, it is known that both organelles may fuse with the plasma membrane and participate in the transport of lipid compounds and proteins to the cell surface (1, 44, 45). Moreover, the late endosomes of dendritic cells are involved in the transport of major histocompatibility complex class II (MHC II) molecules to the plasma membrane upon stimulation by an extracellular stimulus (10, 28, 55). The mechanism of this process is not completely understood but seems to involve a stimulation-dependent transformation of MHC II-containing MVBs into tubular-like structures extending into the periphery. Subsequent fusion of the tubules or of vesicles budding from the tubules with the plasma membrane results in the surface expression of MHC II (28). VP40 is found in tubular structures emanating from the MVBs that are highly similar to tubular structures emerging from MVBs during the surface transport of MHC II molecules (28). The formation of tubular extensions from late endosomes was also shown during the course of trafficking of proteins that participate in intracellular cholesterol transport (39, 64, 65). Tubular-like extensions of late endosomes and homotypic fusion events (42) might explain the formation of VP40 spots with polymorphic shapes and sizes.

The interaction of viral proteins with the late endosomes has been detected before. The replication of mouse hepatitis virus, for example, takes place at late endosomal membranes (56). Furthermore, human cytomegalovirus particles occasionally bud into MVBs, and the viral chemokine receptor-like proteins (UL33 and US27) have been detected in MVBs as well (14). A

recent study demonstrated that infectious human immunodeficiency virus type 1 (HIV-1) particles are assembled in late endosomes of primary macrophages (41).

At the late endosomal compartment, a complex protein machinery drives the sorting of plasma membrane receptors into internal vesicles that bud into the lumen of the endosome (2, 3, 26). This process is crucial for the proper maintenance of receptor density at the plasma membrane and seems to be mechanistically similar to the budding of viruses (4, 18). A connection between the inward budding of endosomal vesicles and the budding process of viruses emerged when it was found that TSG101, a cellular protein that is part of the protein sorting machinery in the late endosome, is required for HIV-1 budding. TSG101 exerts its effect on the budding of HIV-1 by an interaction with the late domain of the viral protein Gag (18). Moreover, the efficient egress of Ebola virus-like particles induced by the Ebola virus matrix protein VP40 was also dependent on an interaction with TSG101 (34). These results suggest that viral proteins might recruit parts of the machinery that normally mediates the invagination of the MVBs to the sites of virus budding at the plasma membrane. However, MARV budding must use a different pathway, since MARV VP40 lacks the PT/SAP motif that is recognized by TSG101 (57). Notably, the majority of M proteins in viruses of the order *Mononegavirales* lack the PT/SAP motif as well. The detected association of MARV VP40 with the late endosome might enable the virus to recruit parts of the endosomal budding machinery to the plasma membrane without a direct interaction with TSG101. Besides the PT/SAP motif, another short peptide motif, PPxY, was shown to contribute to the budding of Ebola virus VP40 (22, 23, 33). This motif is also present in MARV VP40. PPxY motifs interact specifically with WW domains such as that contained in the ubiquitin ligase Nedd4. Indeed, an interaction of Ebola virus VP40 with Nedd4 which is mediated by the PPxY motif and is essential for the budding of virus-like particles has been detected (54, 61). The role of the PPxY motif with MARV VP40 is unclear so far. Substitution mutations of the motif did not lead to a change in the intracellular distribution of VP40 but to a reduction of the release of VP40 in virus-like particles from the cells (unpublished data).

Recently, Bild and colleagues published a study showing that the signal transducer and activator of transcription Stat 3 is transported from the plasma membrane to the nucleus by endocytic vesicles. The process seemed to end up in perinuclear structures before the protein was released by an unknown mechanism into the nucleus (8). Thus, it appears that the exploitation of the endosomal system might be a common mechanism for carrying cytosolic cargo proteins to target sites.

Taken together, the data from the present study highlight a novel intracellular pathway for a viral matrix protein that requires interactions with several cellular membrane structures, particularly the late endosome, for its transport to the plasma membrane. Since viruses mostly exploit existing cellular pathways, it is conceivable that cytosolic cellular proteins use the retrograde late endosomal route for membrane-associated transport as well.

ACKNOWLEDGMENTS

We thank Yoshihiro Kawaoka for providing the vector pCAGGS, Michael Weik for constructing modified pCAGGS, and Stuart Nichol, Centers for Disease Control and Prevention, Atlanta, Ga., for providing a monoclonal antibody against VP40. We thank Hans-Dieter Klenk, Michael Schrader, and Beate Sodeik for critically reading the manuscript, for helpful comments, and for fruitful discussions.

This work was supported by the Deutsche Forschungsgemeinschaft (SFB 593, TP B3, and SFB 535, TP B9) and by the "Hochschulwissenschaftsprogramm" of the Land Hessen and the University of Marburg (Sandra Bamberg).

REFERENCES

1. **Andrews, N. W.** 2002. Lysosomes and the plasma membrane: trypanosomes reveal a secret relationship. J. Cell Biol. **158:**389–394.
2. **Babst, M., D. J. Katzmann, E. J. Estepa-Sabal, T. Meerloo, and S. D. Emr.** 2002. ESCRT-III: an endosome-associated heterooligomeric protein complex required for MVB sorting. Dev. Cell **3:**271–282.
3. **Babst, M., D. J. Katzmann, W. B. Snyder, B. Wendland, and S. D. Emr.** 2002. Endosome-associated complex, ESCRT-II, recruits transport machinery for protein sorting at the multivesicular body. Dev. Cell **3:**283–289.
4. **Babst, M., G. Odorizzi, E. J. Estepa, and S. D. Emr.** 2000. Mammalian tumor susceptibility gene 101 (TSG101) and the yeast homologue, Vps23p, both function in late endosomal trafficking. Traffic **1:**248–258.
5. **Becker, S., H.-D. Klenk, and E. Mühlberger.** 1996. Intracellular transport and processing of the Marburg virus surface protein in vertebrate and insect cells. Virology **225:**145–155.
6. **Becker, S., C. Rinne, U. Hofsass, H.-D. Klenk, and E. Mühlberger.** 1998. Interactions of Marburg virus nucleocapsid proteins. Virology **249:**406–417.
7. **Bergmann, J. E., and P. J. Fusco.** 1988. The M protein of vesicular stomatitis virus associates specifically with the basolateral membranes of polarized epithelial cells independently of the G protein. J. Cell Biol. **107:**1707–1715.
8. **Bild, A. H., J. Turkson, and R. Jove.** 2002. Cytoplasmic transport of Stat3 by receptor-mediated endocytosis. EMBO J. **21:**3255–3263.
9. **Cathomen, T., B. Mrkic, D. Spehner, R. Drillien, R. Naef, J. Pavlovic, A. Aguzzi, M. A. Billeter, and R. Cattaneo.** 1998. A matrix-less measles virus is infectious and elicits extensive cell fusion: consequences for propagation in the brain. EMBO J. **17:**3899–3908.
10. **Chow, A., D. Toomre, W. Garrett, and I. Mellman.** 2002. Dendritic cell maturation triggers retrograde MHC class II transport from lysosomes to the plasma membrane. Nature **418:**988–994.
11. **Dean, R. T., W. Jessup, and C. R. Roberts.** 1984. Effects of exogenous amines on mammalian cells, with particular reference to membrane flow. Biochem. J. **217:**27–40.
12. **Feldmann, H., and H.-D. Klenk.** 1996. Marburg and Ebola viruses. Adv. Virus Res. **47:**1–52.
13. **Ford, T., J. Graham, and D. Rickwood.** 1994. Iodixanol: a nonionic isoosmotic centrifugation medium for the formation of self-generated gradients. Anal. Biochem. **220:**360–366.
14. **Fraile-Ramos, A., A. Pelchen-Matthews, T. N. Kledal, H. Browne, T. W. Schwartz, and M. Marsh.** 2002. Localization of HCMV UL33 and US27 in endocytic compartments and viral membranes. Traffic **3:**218–232.
15. **Fuerst, T. R., E. G. Niles, F. W. Studier, and B. Moss.** 1986. Eukaryotic transient-expression system based on recombinant vaccinia virus that synthesizes bacteriophage T7 RNA polymerase. Proc. Natl. Acad. Sci. USA **83:**8122–8126.
16. **Funke, C., S. Becker, H. Dartsch, H.-D. Klenk, and E. Mühlberger.** 1995. Acylation of the Marburg virus glycoprotein. Virology **208:**289–297.
17. **Garoff, H., R. Hewson, and D. J. Opstelten.** 1998. Virus maturation by budding. Microbiol. Mol. Biol. Rev. **62:**1171–1190.
18. **Garrus, J. E., U. K. von Schwedler, O. W. Pornillos, S. G. Morham, K. H. Zavitz, H. E. Wang, D. A. Wettstein, K. M. Stray, M. Cote, R. L. Rich, D. G. Myszka, and W. I. Sundquist.** 2001. Tsg101 and the vacuolar protein sorting pathway are essential for HIV-1 budding. Cell **107:**55–65.
19. **Grindstaff, K. K., C. Yeaman, N. Anandasabapathy, S. C. Hsu, E. Rodriguez-Boulan, R. H. Scheller, and W. J. Nelson.** 1998. Sec6/8 complex is recruited to cell-cell contacts and specifies transport vesicle delivery to the basal-lateral membrane in epithelial cells. Cell **93:**731–740.
20. **Gruenberg, J.** 2001. The endocytic pathway: a mosaic of domains. Nat. Rev. Mol. Cell Biol. **2:**721–730.
21. **Harty, R. N., M. E. Brown, J. P. McGettigan, G. Wang, H. R. Jayakar, J. M. Huibregtse, M. A. Whitt, and M. J. Schnell.** 2001. Rhabdoviruses and the cellular ubiquitin-proteasome system: a budding interaction. J. Virol. **75:**10623–10629.
22. **Harty, R. N., M. E. Brown, G. Wang, J. Huibregtse, and F. P. Hayes.** 2000. A PPxY motif within the VP40 protein of Ebola virus interacts physically and functionally with a ubiquitin ligase: implications for filovirus budding. Proc. Natl. Acad. Sci. USA **97:**13871–13876.
23. **Harty, R. N., J. Paragas, M. Sudol, and P. Palese.** 1999. A proline-rich motif within the matrix protein of vesicular stomatitis virus and rabies virus inter-

acts with WW domains of cellular proteins: implications for viral budding. J. Virol. **73:**2921–2929.
24. **Hopkins, C. R., A. Gibson, M. Shipman, and K. Miller.** 1990. Movement of internalized ligand-receptor complexes along a continuous endosomal reticulum. Nature **346:**335–339.
25. **Jasenosky, L. D., G. Neumann, I. Lukashevich, and Y. Kawaoka.** 2001. Ebola virus VP40-induced particle formation and association with the lipid bilayer. J. Virol. **75:**5205–5214.
26. **Katzmann, D. J., M. Babst, and S. D. Emr.** 2001. Ubiquitin-dependent sorting into the multivesicular body pathway requires the function of a conserved endosomal protein sorting complex, ESCRT-I. Cell **106:**145–155.
27. **Klausner, R. D., J. G. Donaldson, and J. Lippincott-Schwartz.** 1992. Brefeldin A: insights into the control of membrane traffic and organelle structure. J. Cell Biol. **116:**1071–1080.
28. **Kleijmeer, M., G. Ramm, D. Schuurhuis, J. Griffith, M. Rescigno, P. Ricciardi-Castagnoli, A. Y. Rudensky, F. Ossendorp, C. J. Melief, W. Stoorvogel, and H. J. Geuze.** 2001. Reorganization of multivesicular bodies regulates MHC class II antigen presentation by dendritic cells. J. Cell Biol. **155:**53–63.
29. **Kobasa, D., M. E. Rodgers, K. Wells, and Y. Kawaoka.** 1997. Neuraminidase hemadsorption activity, conserved in avian influenza A viruses, does not influence viral replication in ducks. J. Virol. **71:**6706–6713.
30. **Kolesnikova, L., H. Bugany, H.-D. Klenk, and S. Becker.** 2002. VP40, the matrix protein of Marburg virus, is associated with membranes of the late endosomal compartment. J. Virol. **76:**1825–1838.
31. **Kolesnikova, L., E. Mühlberger, E. Ryabchikova, and S. Becker.** 2000. Ultrastructural organization of recombinant Marburg virus nucleoprotein: comparison with Marburg virus inclusions. J. Virol. **74:**3899–3904.
32. **Lenard, J.** 1996. Negative-strand virus M and retrovirus MA proteins: all in a family? Virology **216:**289–298.
33. **Licata, J. M., M. Simpson-Holley, N. T. Wright, Z. Han, J. Paragas, and R. N. Harty.** 2003. Overlapping motifs (PTAP and PPEY) within the Ebola virus VP40 protein function independently as late budding domains: involvement of host proteins tsg101 and vps-4. J. Virol. **77:**1812–1819.
34. **Martin-Serrano, J., T. Zang, and P. D. Bieniasz.** 2001. HIV-1 and Ebola virus encode small peptide motifs that recruit Tsg101 to sites of particle assembly to facilitate egress. Nat. Med. **7:**1313–1319.
35. **Maxfield, F. R.** 1982. Weak bases and ionophores rapidly and reversibly raise the pH of endocytic vesicles in cultured mouse fibroblasts. J. Cell Biol. **95:**676–681.
36. **Mebatsion, T., F. Weiland, and K. K. Conzelmann.** 1999. Matrix protein of rabies virus is responsible for the assembly and budding of bullet-shaped particles and interacts with the transmembrane spike glycoprotein G. J. Virol. **73:**242–250.
37. **Modrof, J., C. Moritz, L. Kolesnikova, T. Konakova, B. Hartlieb, A. Randolf, E. Mühlberger, and S. Becker.** 2001. Phosphorylation of Marburg virus VP30 at serines 40 and 42 is critical for its interaction with NP inclusions. Virology **287:**171–182.
38. **Mollenhauer, H. H., D. J. Morre, and L. D. Rowe.** 1990. Alteration of intracellular traffic by monensin; mechanism, specificity and relationship to toxicity. Biochim. Biophys. Acta **1031:**225–246.
39. **Neufeld, E. B., A. T. Remaley, S. J. Demosky, J. A. Stonik, A. M. Cooney, M. Comly, N. K. Dwyer, M. Zhang, J. Blanchette-Mackie, S. Santamarina-Fojo, and H. B. Brewer, Jr.** 2001. Cellular localization and trafficking of the human ABCA1 transporter. J. Biol. Chem. **276:**27584–27590.
40. **Niwa, H., K. Yamamura, and J. Miyazaki.** 1991. Efficient selection for high-expression transfectants with a novel eukaryotic vector. Gene **108:**193–199.
41. **Pelchen-Matthews, A., B. Kramer, and M. Marsh.** 2003. Infectious HIV-1 assembles in late endosomes in primary macrophages. J. Cell Biol. **162:**443–455.
42. **Piper, R. C., and J. P. Luzio.** 2001. Late endosomes: sorting and partitioning in multivesicular bodies. Traffic **2:**612–621.
43. **Plonne, D., I. Cartwright, W. Linss, R. Dargel, J. M. Graham, and J. A. Higgins.** 1999. Separation of the intracellular secretory compartment of rat liver and isolated rat hepatocytes in a single step using self-generating gradients of iodixanol. Anal. Biochem. **276:**88–96.
44. **Reddy, A., E. V. Caler, and N. W. Andrews.** 2001. Plasma membrane repair is mediated by Ca(2+)-regulated exocytosis of lysosomes. Cell **106:**157–169.
45. **Rodriguez, A., P. Webster, J. Ortego, and N. W. Andrews.** 1997. Lysosomes behave as Ca2+-regulated exocytic vesicles in fibroblasts and epithelial cells. J. Cell Biol. **137:**93–104.
46. **Rouille, Y., W. Rohn, and B. Hoflack.** 2000. Targeting of lysosomal proteins. Semin. Cell Dev. Biol. **11:**165–171.
47. **Sanderson, C. M., H. H. Wu, and D. P. Nayak.** 1994. Sendai virus M protein binds independently to either the F or the HN glycoprotein in vivo. J. Virol. **68:**69–76.
48. **Schmitt, A. P., B. He, and R. A. Lamb.** 1999. Involvement of the cytoplasmic domain of the hemagglutinin-neuraminidase protein in assembly of the paramyxovirus simian virus 5. J. Virol. **73:**8703–8712.
49. **Schnell, M. J., L. Buonocore, E. Boritz, H. P. Ghosh, R. Chernish, and J. K. Rose.** 1998. Requirement for a non-specific glycoprotein cytoplasmic domain sequence to drive efficient budding of vesicular stomatitis virus. EMBO J. **17:**1289–1296.
50. **Smith, D. H., B. K. Johnson, M. Isaacson, R. Swanapoel, K. M. Johnson, M. Killey, A. Bagshawe, T. Siongok, and W. K. Keruga.** 1982. Marburg-virus disease in Kenya. Lancet **i:**816–820.
51. **Steinman, R. M., and Z. A. Cohn.** 1972. The interaction of soluble horseradish peroxidase with mouse peritoneal macrophages in vitro. J. Cell Biol. **55:**186–204.
52. **Sutter, G., M. Ohlmann, and V. Erfle.** 1995. Non-replicating vaccinia vector efficiently expresses bacteriophage T7 RNA polymerase. FEBS Lett. **371:**9–12.
53. **Timmins, J., S. Scianimanico, G. Schoehn, and W. Weissenhorn.** 2001. Vesicular release of Ebola virus matrix protein VP40. Virology **283:**1–6.
54. **Timmins, J., G. Schoehn, S. Ricard-Blum, S. Scianimanico, T. Vernet, R. W. Ruigrok, and W. Weissenhorn.** 2003. Ebola virus matrix protein VP40 interaction with human cellular factors Tsg101 and Nedd4. J. Mol. Biol. **326:**493–502.
55. **Turley, S. J., K. Inaba, W. S. Garrett, M. Ebersold, J. Unternaehrer, R. M. Steinman, and I. Mellman.** 2000. Transport of peptide-MHC class II complexes in developing dendritic cells. Science **288:**522–527.
56. **van der Meer, Y., E. J. Snijder, J. C. Dobbe, S. Schleich, M. R. Denison, W. J. Spaan, and J. K. Locker.** 1999. Localization of mouse hepatitis virus nonstructural proteins and RNA synthesis indicates a role for late endosomes in viral replication. J. Virol. **73:**7641–7657.
57. **VerPlank, L., F. Bouamr, T. J. LaGrassa, B. Agresta, A. Kikonyogo, J. Leis, and C. A. Carter.** 2001. Tsg101, a homologue of ubiquitin-conjugating (E2) enzymes, binds the L domain in HIV type 1 Pr55(Gag). Proc. Natl. Acad. Sci. USA **98:**7724–7729.
58. **Volchkov, V. E., H. Feldmann, V. A. Volchkova, and H.-D. Klenk.** 1998. Processing of the Ebola virus glycoprotein by the proprotein convertase furin. Proc. Natl. Acad. Sci. USA **95:**5762–5767.
59. **Weibel, E. R.** 1972. The value of stereology in analysing structure and function of cells and organs. J. Microsc. **95:**3–13.
60. **World Health Organization.** 1999. Marburg fever in the Democratic republic of the Congo. Wkly. Epidemiol. Rec. **74:**145.
61. **Yasuda, J., M. Nakao, Y. Kawaoka, and H. Shida.** 2003. Nedd4 regulates egress of Ebola virus-like particles from host cells. J. Virol. **77:**9987–9992.
62. **Yeaman, C., K. K. Grindstaff, J. R. Wright, and W. J. Nelson.** 2001. Sec6/8 complexes on trans-Golgi network and plasma membrane regulate late stages of exocytosis in mammalian cells. J. Cell Biol. **155:**593–604.
63. **Zhang, J., and R. A. Lamb.** 1996. Characterization of the membrane association of the influenza virus matrix protein in living cells. Virology **225:**255–266.
64. **Zhang, M., N. K. Dwyer, D. C. Love, A. Cooney, M. Comly, E. Neufeld, P. G. Pentchev, E. J. Blanchette-Mackie, and J. A. Hanover.** 2001. Cessation of rapid late endosomal tubulovesicular trafficking in Niemann-Pick type C1 disease. Proc. Natl. Acad. Sci. USA **98:**4466–4471.
65. **Zhang, M., P. Liu, N. K. Dwyer, L. K. Christenson, T. Fujimoto, F. Martinez, M. Comly, J. A. Hanover, E. J. Blanchette-Mackie, and J. F. Strauss III.** 2002. MLN64 mediates mobilization of lysosomal cholesterol to steroidogenic mitochondria. J. Biol. Chem. **277:**33300–33310.